



Supplementary Materials for

Profiling risk and sustainability in coastal deltas of the world

Z. D. Tessler,* C. J. Vörösmarty, M. Grossberg, I. Gladkova, H. Aizenman, J. P. M. Syvitski, E. Foufoula-Georgiou

*Corresponding author. E-mail: ztessler@ccny.cuny.edu

Published 7 August 2015, *Science* **349**, 638 (2015)

DOI: [10.1126/science.aab3574](https://doi.org/10.1126/science.aab3574)

This PDF file includes:

Materials and Methods

Figs. S1 to S4

Tables S1 to S3

Materials and Methods:

Risk framework

The delta risk framework used here is based on a commonly used formalism for expected loss (17, 22, 23). For a given type and intensity of *hazard*, represented as a random variable h , we define the *exposure*, $E(h)$, as the number of people exposed to hazardous conditions, and the *vulnerability*, $V(h)$, as the fraction of the exposed population who are harmed by this hazard. Then the total *risk*, R , or expected loss, to a population from a range of various types and intensities of hazards, each with probability $H(h)$, over some time period is

$$R = \sum_h H(h)E(h)V(h). \quad \text{Eq. S1}$$

Considering only a single representative hazard class and differentiating, the rate of change of risk is the sum of three terms, each the product of the change in one risk factor with the current state of the other two factors:

$$R' = H'EV + HE'V + HEV' \quad \text{Eq. S2}$$

where the prime notation indicates a rate of change. In this study, we consider only the rate of increase in R due to change in exposure from relative sea level rise, treating H and V as constant in time:

$$R' = HE'V. \quad \text{Eq. S3}$$

The factors H , E' and V can, in theory, be estimated or measured directly. However, this is currently impractical at the global scale. Estimating frequency distributions of hazard events directly requires long time series of historical events for each delta. While global coverage of tropical cyclones and offshore storm systems is available over the satellite record, historical river discharge data for many systems outside the United States and Europe are frequently incomplete. Direct measurement of population exposure and vulnerability to flooding events requires a long and detailed historical record to adequately sample the domain of possible flood conditions and their impacts on delta communities. These data do not exist over much of the globe, particularly prior to satellite-based flood detection methods. The best available historical flood database, the Dartmouth Flood Observatory, has records only from 1985 (34).

Rather than reconstructing population exposure from historical events, exposure estimates can also be made using high resolution digital elevation models to map populations exposed to fluvial or coastal floods of a given magnitude. Elevation maps with this level of detail currently exists only for a select few delta systems. LIDAR mapping of the Rhine Delta (*Actueel Hoogtebestand Nederland*), for instance, is available at high enough resolution to capture necessary fine details, but similar data do not exist for most of the world's deltas. We can nonetheless say with a high degree of certainty that regardless of the true population exposure at

a given moment in time, land subsidence and sea level rise directly contribute to increases in exposure.

Due to the challenges of measuring these risk components directly, the construction of indices based on mature, global datasets as proxies for direct measurement is a starting point for evaluation and comparison of the changing risk profile of delta systems. We propose that these empirical indices, indicated by the circumflex symbols, are functionally related to each of the factors in *Eq. S3*:

$$\hat{H} = f(H) \quad \text{Eq. S4}$$

$$\hat{E}' = g(E') \quad \text{Eq. S5}$$

$$\hat{V} = h(V). \quad \text{Eq. S6}$$

The risk index is estimated as a function of the empirical indices:

$$\hat{R}' = \hat{H}\hat{E}'\hat{V} \quad \text{Eq. S7}$$

where \hat{H} is the Hazardous Event Index (HEI), \hat{E}' is the Anthropogenic Conditioning Index (ACI), and \hat{V} is the Investment Deficit Index (IDI). In the main paper, the use of circumflex symbols is dropped, with the understanding that all results are for the estimated quantities.

Index construction

These three risk component indices are constructed from a suite of indicators deriving from the local delta, the upstream watershed, and the offshore environment. Similar indicator suites have been shown to relate well with observed relative sea level rise (35). Additionally, each individual indicator has documented effects on delta processes that control relative sea level rise (Table S1). All *ACI* indicators have been shown to lead directly or indirectly to increased delta subsidence and/or loss of protective coastal wetlands through upstream, local, and offshore processes. The full Anthropogenic Conditioning Index, described below, compares well with observed relative sea level rise for systems where estimates are available (Fig. S1). The positive functional relationship between the index and relative sea level rise estimates supports the use of the index in other deltas where relative sea level rise observations are not available.

Deltas included in this study are a superset of those considered earlier (5, 8), with spatial extents based on (8), and extended to additional deltas based on SRTM topography for elevation and relief, river network bifurcations to identify the delta apex, presence of fluvial-sourced soils, and visual inspection of land cover from Landsat to identify distinctive vegetation patterns (Table S2). For each delta indicator, data is first extracted from global datasets over delta extents (Table S2). For basin indicators, data is aggregated over all river basins in the Simulated Topological Network (STN06) (36) digital river network with an outlet within the delta. For most deltas, these upstream basins consist of one large watershed and several small to medium watersheds. The Ganges-Brahmaputra is an important exception to this, where several large basins contribute to a single delta.

Global delta population is estimated by aggregating GRUMPv1 population data, circa 2000 (21), over the 48 delta extents. Delta population in 2000 is estimated as 286 million people. We apply a globally constant population growth rate between 2000 and 2015 and obtain an estimate of 341 million people within the mapped delta extent in 2015. Upstream basin populations estimates of 3.5 billion people are made in a similar manner.

Given the several orders of magnitude variation in scale across some deltas, we use rank-normalization to reduce the relative influence of outlier deltas. The ranked indicator values are then unity-normalized to reduce distortion introduced by zero-valued raw indicators over several deltas. For instance, while several deltas do not have appreciable oil and gas extraction, they nonetheless each have a non-zero rank. Unity-normalization reduces the indicator value of the lowest ranked delta, or deltas, to zero, and the highest ranked to 1:

$$I_{i,d} = \frac{\hat{I}_{i,d} - \min(\hat{I}_{i,d})}{\max(\hat{I}_{i,d}) - \min(\hat{I}_{i,d})} \quad \text{Eq. S8}$$

where $\hat{I}_{i,d}$ is the ascending rank order over all deltas of indicator i at delta d .

We then derive the Anthropogenic Conditioning Index, ACI_d , for a given delta d , as a weighted mean of each indicator:

$$ACI_d = \frac{\sum_i I_{i,d} w_i}{\sum_i w_i} \quad \text{Eq. S9}$$

where w_i is the weight for a given indicator i , and m is the number of indicator variables. Results in the main paper are presented for equally weighted indicators. This approach enables comparison of each delta to a representative “median delta.”

Indicators include population density in the delta and upstream basin (21), an indirect measure of development and land use change; estimated artificial reservoir volume upstream (37), normalized by mean river discharge, a measure of riverine sediment trapping (6); wetland disconnectivity (20) in the delta and upstream basin, an indicator of agricultural conversion and urbanization of former wetlands; impervious surface fraction (38) in the upstream basin and delta, evidence of development of natural landcover; estimated delta groundwater abstraction in excess of recharge (39), a major component of accelerated delta land subsidence (8); and a petroleum extraction indicator (40), an additional determinant of accelerated delta land subsidence (41). Local sea level rise, with rates estimated from trends in the satellite altimetry record, is the final ACI indicator (Fig. S3). Sea level rise trends were calculated from combined TOPEX/Poseidon, Jason-1, and Jason-2/OSTM sea level fields over the years 1993-2013 (42). The altimetry-based sea level dataset used has not been adjusted for the inverse barometer effect or glacial isostatic adjustment in order to obtain the most accurate estimate of relative sea level rise realized at the coast, rather than only that due to eustatic sea level rise. Sea level rise is taken as the mean value within 100km of the delta coast. In the cases where the closest altimetry data to the coast is greater than 100km from the delta, a preprocessing step is included to extend coastal data landward using a nearest neighbor extrapolation. This was required for the analysis

of 11 deltas. Most of these extrapolations are only a few 0.4 degree pixels, on the order of 100 km, however this method assigns sea level rise trend estimates from the northeastern Mediterranean Sea to the Danube and Dnieper deltas in the Black Sea, for which data is not available in the sea level dataset used here. The assumption of similar trends in the Black Sea and northeastern Mediterranean Sea is supported by regional studies (43).

Correlations between indicator variables can add additional weight to an underlying latent variable in the final index. We find correlations between the delta and upstream population densities, and population density and impervious surface indicator variables in the Anthropogenic Conditioning Index. There are several approaches to handling these correlations when constructing indexes, a primary one being Principal Component Analysis. However, transforming the data by PCA presents several drawbacks. For one, the number of retained dimensions is a tunable parameter that must be chosen. Additionally, the interpretation of the results becomes far more difficult. Here, for instance, we can identify the specific factors that result in a high Anthropogenic Conditioning Index score in the Ganges-Brahmaputra. We use a sensitivity analysis to define the expected risk rank bounds as the relative weights of each indicator variable are allowed to vary. This can be used to see the potential change in rank due to strong correlations, where two correlated indicator variables double-count the underlying latent variable.

The sensitivity analysis was conducted by calculating the resulting index scores for each delta under random selections of indicator weights between 0 and 1. After 10,000 iterations the average of the standard deviation of rank distributions for each delta is 4.08. This is an estimate of the error of the ranking deriving from uncertainty in the correct weighting scheme. The rank-error is greatest for deltas near the center of the index, where differences between delta scores are smallest (Fig. S2). The index score error is particularly high for deltas strongly influenced by only a few indicators (Colorado, Rio Grande, Senegal). For instance, the Rio Grande has very high groundwater extraction and upstream dams, but low population, and therefore is sensitive to the weights for those particular indicators. The standard deviation of rank estimates for the Rio Grande was 7.29, the highest of any delta in the study. Alternative normalizations change the relative ranking of individual deltas, though the broad patterns remain robust. Specifically, ACI rankings drawn from data that was and was not first rank-transformed are well correlated, with $R^2 = 0.84$ and a linear best-fit slope of 0.92, suggesting the uncertainty introduced by different normalization methods is small.

The Ganges-Brahmaputra, the Krishna, and the Godavari deltas are the most strongly perturbed systems in the study, with overall *ACI* scores of 0.79, 0.72, and 0.69, respectively (Fig. S2). In this construction, a score of 1 would indicate a single delta ranked highest for each individual indicator. Our estimates are broadly consistent with expert assessments in the literature, where the Ganges-Brahmaputra, for instance, has been identified as highly stressed both in delta-specific research (44) and comparative qualitative studies (8, 11). The high-latitude, sparsely populated Yukon, Lena, and Mackenzie deltas, well recognized as being under low pressure (5), have index scores of 0.03, 0.10, and 0.13, respectively, with artificial reservoirs upstream and sea level rise being the only appreciable stressors in the Lena and Mackenzie.

The Hazardous Event Index, *HEI*, was constructed in a similar manner as the Anthropogenic Conditioning Index (Figure S3). Four indicators were used: 30-yr discharge and wave energy return levels, tropical cyclone risk, and M_2 tidal amplitude. Return values were estimated by fitting a Generalized Pareto Distribution to daily river discharge entering the delta apex and daily mean wave energy within 150km of the delta. Discharge estimates are from the WBMplus hydrological model, and waves are from a WAVEWATCH III model hindcast (45, 46). Model data were used to obtain a global, consistent database of discharge and wave energy. Return values were standardized by each delta's mean and standard deviation discharge and wave energy for comparison across deltas. Tropical cyclone frequency was obtained from the Global Cyclone Hazard Frequency and Distribution, v1 (1980-2000) dataset (47), taking the mean cyclone frequency score within a 100km zone centered on the delta coast. High tidal amplitude, from the TPXO7.2 inverse tidal solution (48) is taken as an indicator of increased hazard intensity. It has been suggested that coastlines with low tidal amplitude should be considered more at-risk than those with high tidal amplitudes, based on the idea that high tidal amplitude provides a chance that a negative tidal phase will be of great enough magnitude to offset a storm surge, while low tidal amplitude coastlines are always exposed to a near-full storm surge (18, 49). However, we argue here that the damage functions for storm surges are non-linear, particularly in urbanized deltas, and the increased risk due to a storm surge coinciding with a large positive tidal phase is greater than the reduced risk from a storm surge coinciding with a negative tidal phase. Therefore, the larger the tidal amplitude, the greater the potential for very large storm surge heights, and the greater the overall hazard.

The vulnerability, V , reflecting the level of harm derived from flood exposure, is primarily dependent on socio-economic context. Improvements to civil infrastructure, such as building codes, reduce overall vulnerability. We use per-capita GDP (50) within the delta as an indicator of infrastructure quality. On a broader scale, the aggregate GDP within a delta is related to the capacity and possibly the incentive to invest in larger-scale engineered risk-reducing technologies such as dikes and levees, pumping stations, or storm surge barriers. The distinction between these GDP measures reflects the importance of individual and collective risk-reduction strategies. Additionally, we use the Government Effectiveness measure from the World Governance Indicators (51) as a proxy for the capacity to prepare for and respond to a hazardous event. Together, these three indicators are used to construct an Investment Capacity Index (*ICI*) (Fig. S4) and its complement, the Investment Deficit Index, (*IDI*), a proxy for V , calculated as $IDI = (1 - ICI)$.

Risk sensitivity to future investment capacity

It has been suggested that external inputs of energy and financial resources into a delta system is unsustainable due to likely increases in future energy costs (14). We also note that increasing anthropogenic perturbation of the delta system, including the watershed and offshore domains, serves to increase the challenges facing deltas. Over time, we expect both the cost per unit energy input into the delta to rise, as well as the total amount of energy required to maintain a constant level of protection. To test the consequences of both of these factors, we construct a future vulnerability estimate, IDI_F , by reducing the weight of the GDP indicators in the Investment Deficit Index. This discounts the investment reducing capacity from GDP relative to

the Government Effectiveness indicator. The reduction in weight is determined by using projected energy costs 100 years in the future, given current energy and GDP price index growth forecasts (28). The US Energy Information Administration forecasts GDP Price Index growth out to 2040 of 1.8% per year, while the Fuel and Power Wholesale Price Index is forecast to grow at 2.9% per year. The difference between these growth rates represents the forecast real increasing cost of energy. Additional price growth rates based on low or high oil price assumptions provide approximate bounds on the projected growth rate (Table S3). We extend these growth rates out to 100 years for this scenario. The modified Future Investment Deficit Index is used to develop risk profiles for this future scenario in Fig. 2, 3 and 4. The use of a constant, global discounting factor is a simplification as delta-scale economic forecasting is beyond the scope of this study. This simple scenario is not intended as a forecast, but rather to highlight the sensitivity of each delta system to changes in risk components.

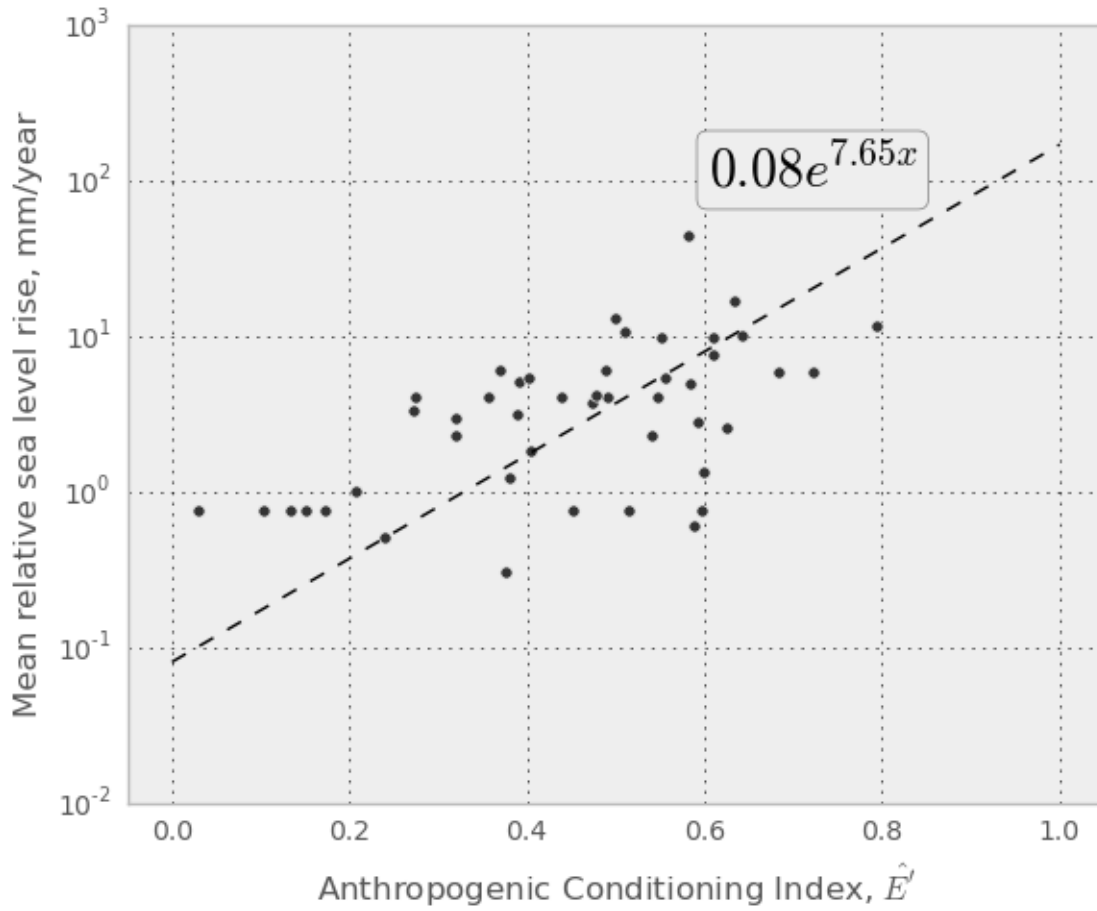


Fig S1: Anthropogenic Conditioning Index, \hat{E}' , versus the average relative sea level rise from estimates in the literature (5, 8). Note vertical logarithmic scale. The best-fit parameters are estimated by orthogonal distance regression. R in log-linear space is 0.56.

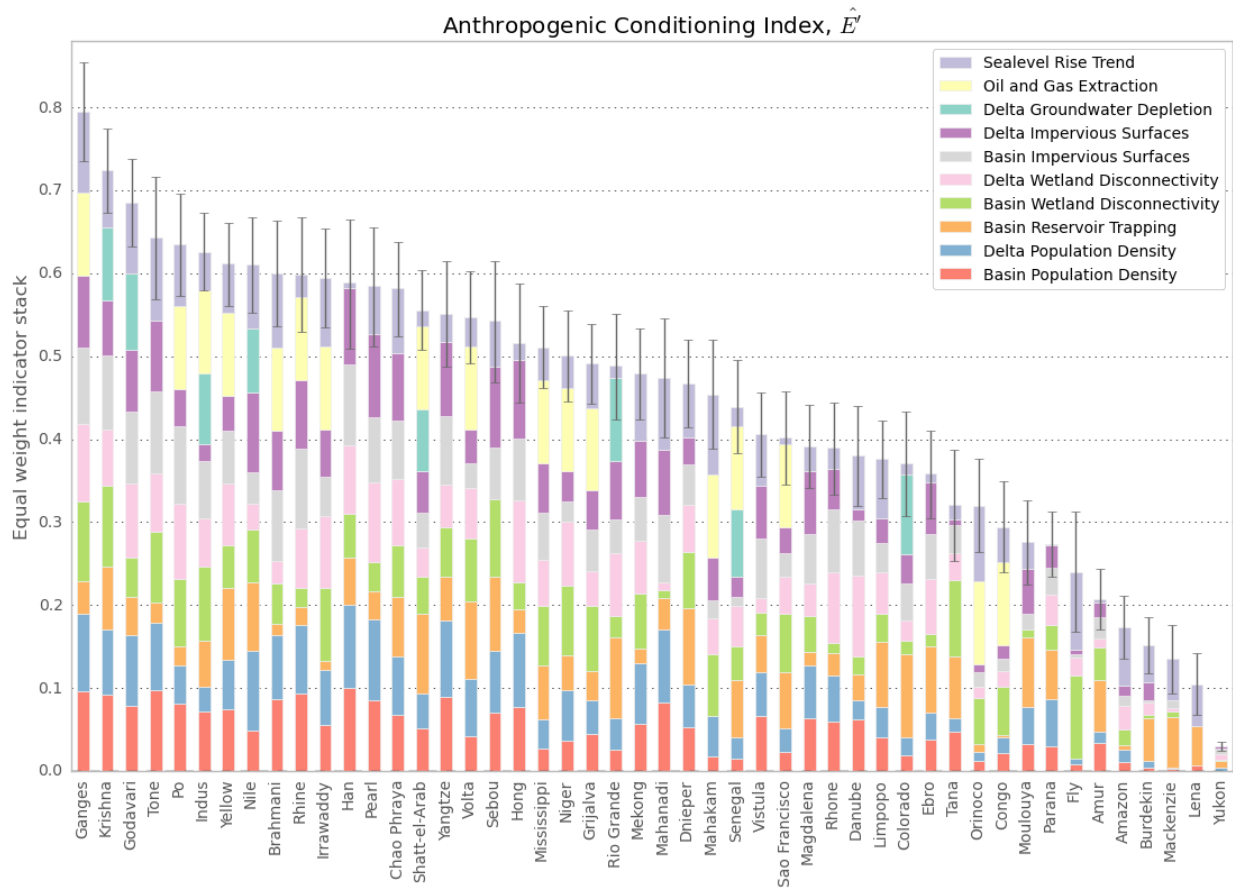


Fig S2: Anthropogenic Conditioning Index, ACI , for the 48 deltas in this study. ACI is constructed as an equal weighted average of 10 indicators, 5 from the local delta, 4 from the upstream contributing river basins, and one from offshore. For each indicator, the deltas are ranked, and the rank values are then unity normalized. Missing data is assigned the median rank. Indicator normalizations are described in the Supplemental Materials. Errorbars show one standard deviation of indicator stack for 10,000 random selections of indicator weights.

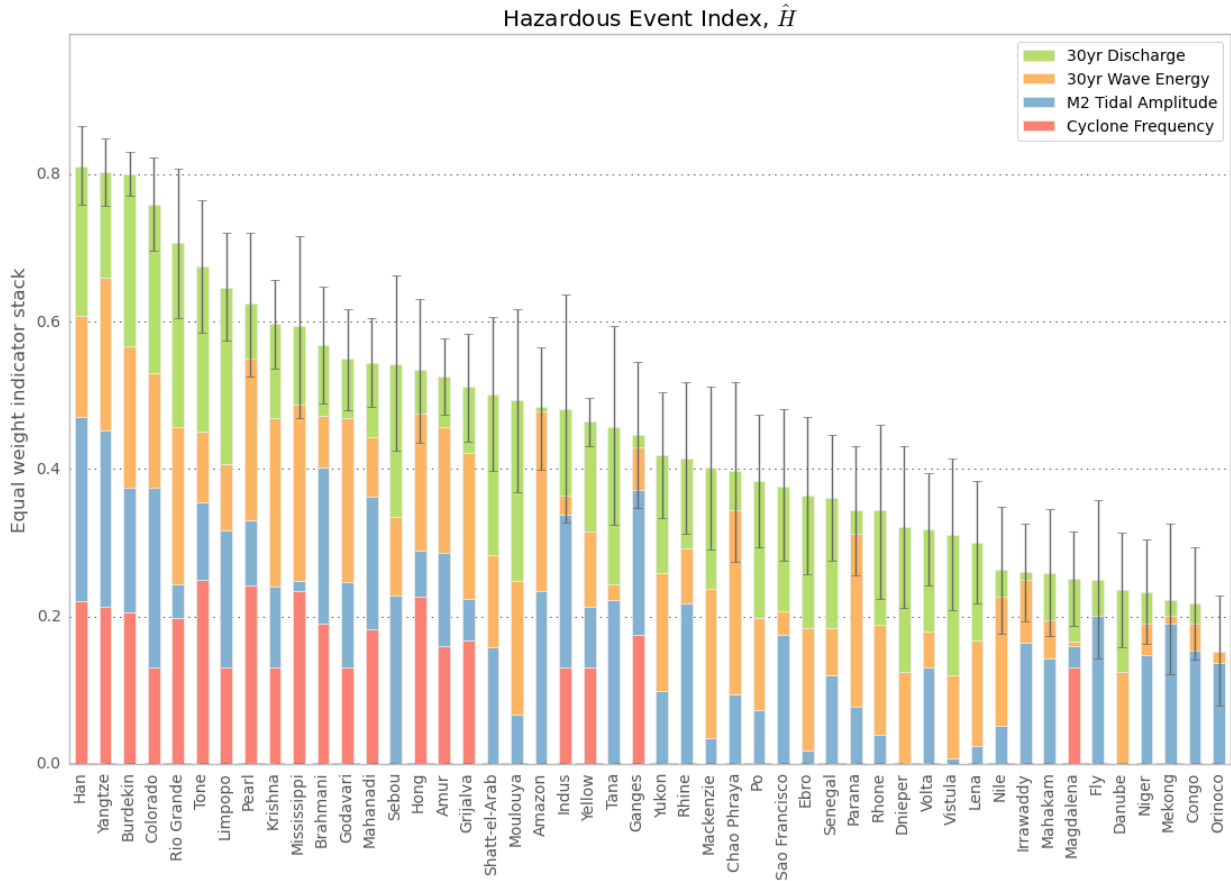


Fig S3: As Fig. S2, but for the Hazardous Event Index, HEI , for the 48 deltas in this study. Indicator variables include measures of extreme river discharge and wave energy, M_2 tidal amplitude, and tropical cyclone frequency. Errorbars show one standard deviation of indicator stack for 10,000 random selections of indicator weights.

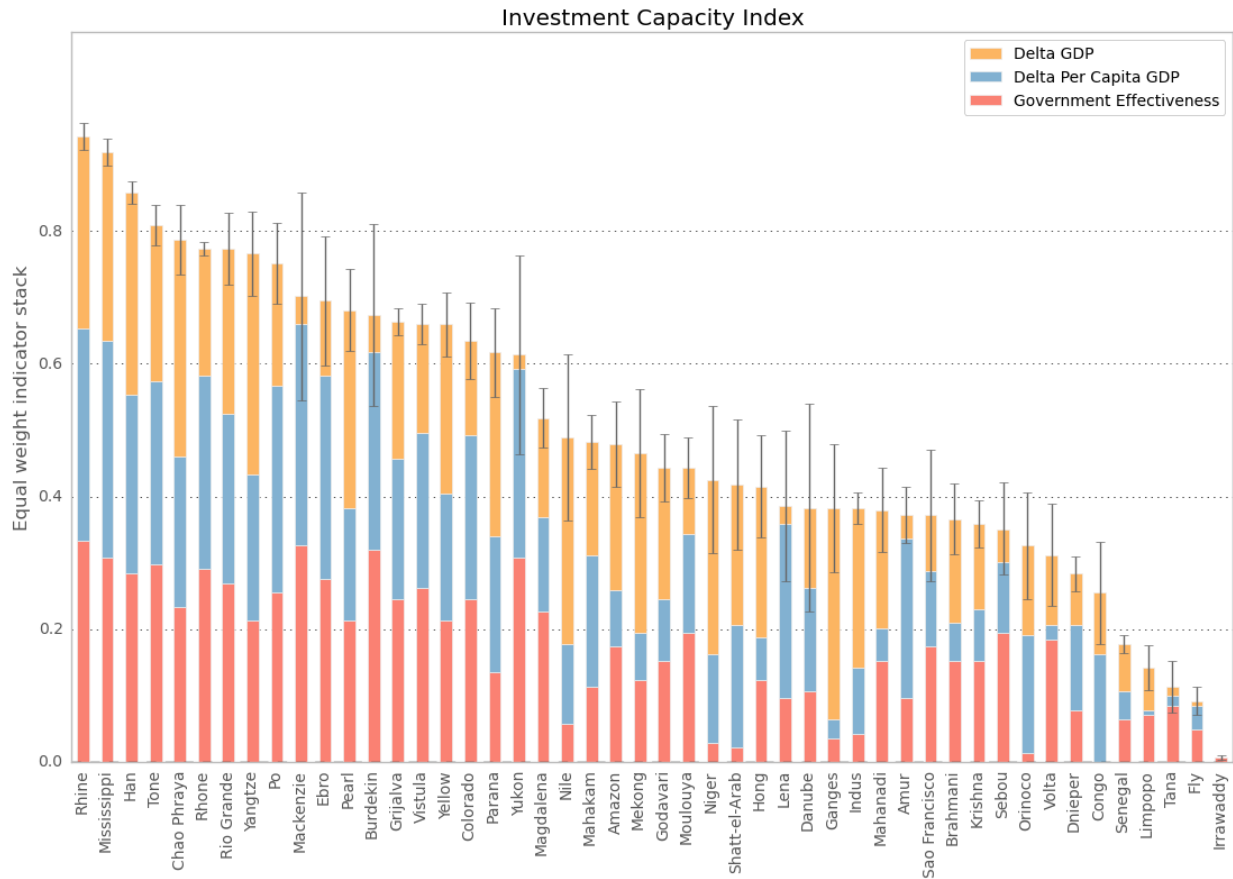
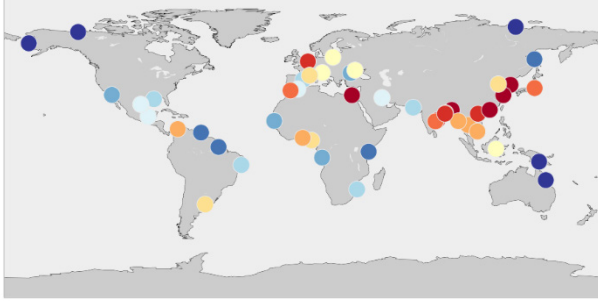
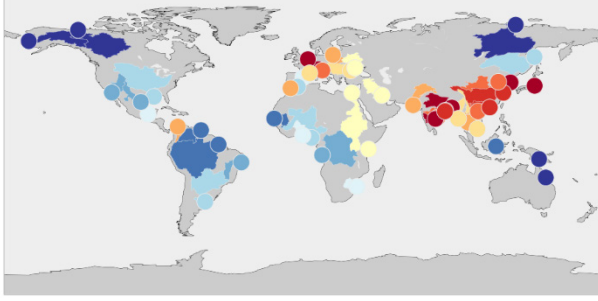
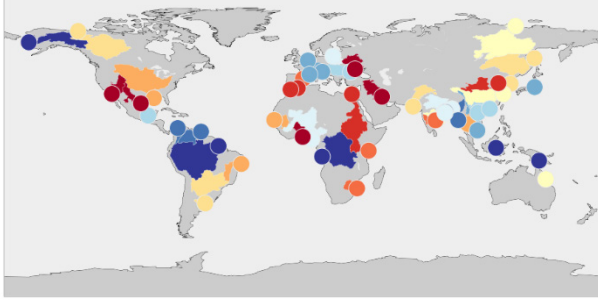
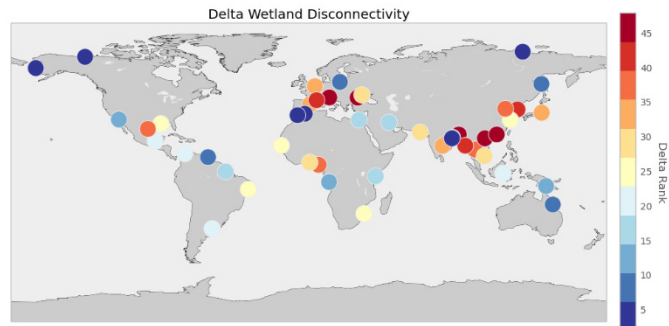


Fig S4: As Fig. S2, but for the Investment Capacity Index (*ICI*), for the 48 deltas in this study. The Investment Deficit Index is estimated from this as $IDI = (1 - ICI)$. Indicator variables are aggregate delta GDP and delta per capita GDP (*50*), and the Government Effectiveness score from the Worldwide Governance Indicators (*51*). Index is constructed from an equal weighting of indicators. Errorbars show one standard deviation of indicator stack for 10,000 random selections of indicator weights.

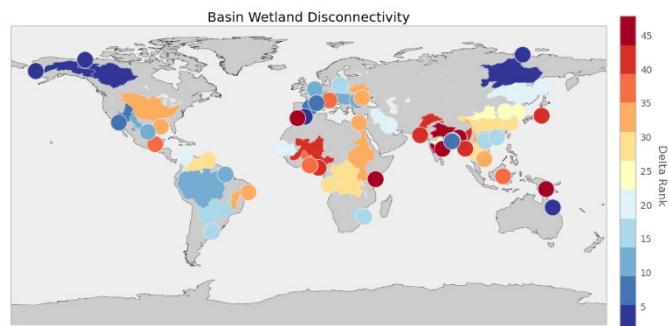
Indicator	Map	Description
<p data-bbox="73 573 316 640">Population Density (ACI Component)</p>	<div style="display: flex; flex-direction: column; align-items: center;"> <div style="display: flex; justify-content: space-between; width: 100%;"> Delta Delta Population Density </div>  <div style="display: flex; justify-content: space-between; width: 100%;"> Basin Basin Population Density </div>  </div>	<p data-bbox="1214 275 1539 779">Population density is considered as an indirect indicator of delta development and pressure on natural ecosystems. Population density is from the year 2000, averaged separately over the delta and all contributing river basins. Original data is from GRUMP v1, at 30 arc sec spatial resolution (21).</p>
<p data-bbox="73 1262 316 1367">Reservoir Volume Sediment Trapping (ACI Component)</p>	<div style="display: flex; flex-direction: column; align-items: center;"> <div style="display: flex; justify-content: space-between; width: 100%;"> Basin Basin Reservoir Trapping </div>  </div>	<p data-bbox="1214 951 1539 1675">Estimated reservoir sediment trapping coefficient (37). Upstream reservoirs and dams trap sediment, reducing the fluvial sediment flux to the delta, and contributing to reduced aggregation and increased relative sea level rise. Total volume of large reservoirs in each basin determined from the GWSP-GRAND (Global Reservoir and Dam Database), normalized by WBMplus modeled mean river discharge exiting the basin.</p>

Wetland
Disconnectivity
(ACI Component)

Delta



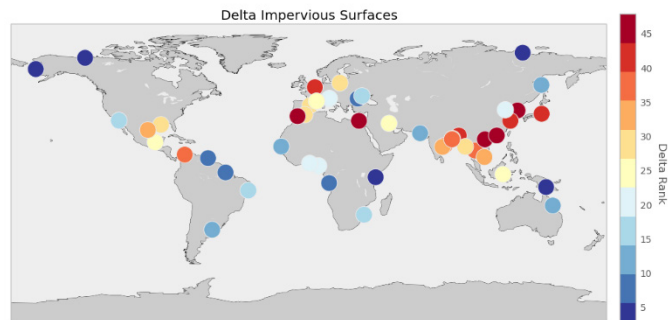
Basin



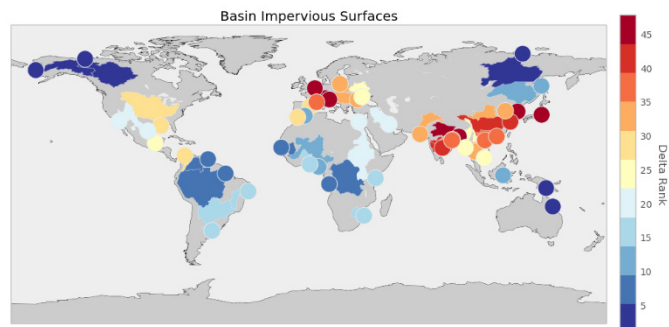
Wetland disconnectivity is an estimate of wetland area that has been drained or otherwise converted for human use (20). This is an indirect measure of loss of natural wetland ecosystems. Calculated by measuring the area classified as non-lake or reservoir wetlands in the Global Lakes and Wetland Database, coincident with areas classified as cropland by Boston University's MODIS land cover classification for year 2000, or identified as impervious surface area by the NOAA-ISA dataset

Impervious Surface
Area
(ACI Component)

Delta

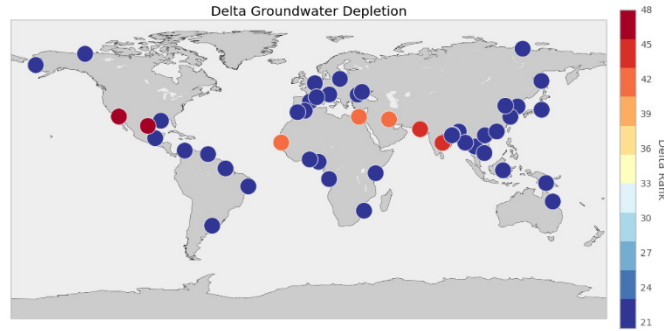


Basin



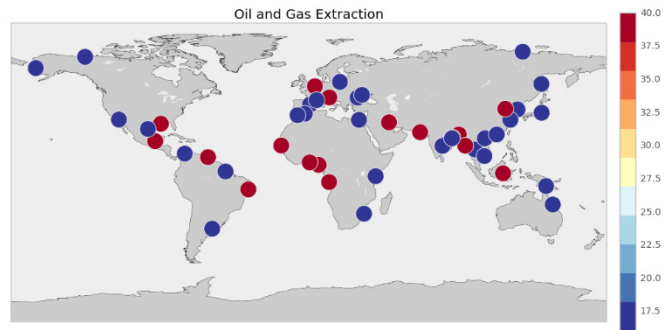
Mean impervious surface area over deltas and their upstream contributing basins, circa 2000-1 (38). Impervious surface areas consist of man-made, constructed surfaces such as buildings and roads. These surfaces are prevented from natural buildup by sediment deposition and are more susceptible to net land subsidence.

Groundwater Depletion
(ACI Component) Delta



Unsustainable groundwater depletion over delta areas, circa 2000 (39). Groundwater extraction from delta sediments reduces pore pressure and accelerates land subsidence. It can also contribute to salt water intrusion from the coast. This is estimated using downscaled, country level statistics of groundwater abstraction, augmented with hydrological model estimates of gross crop water demand, available surface water, and groundwater recharge. Missing data due to lack of national data was taken as zero.

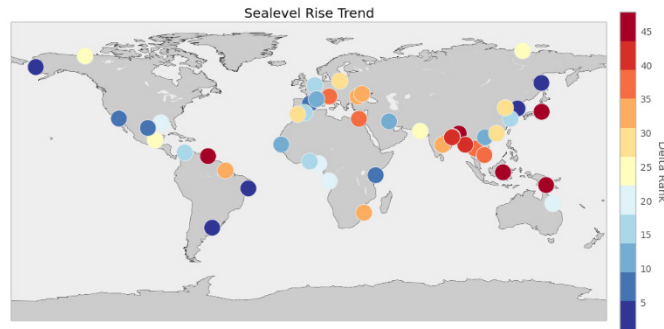
Oil and Gas Extraction
(ACI Component) Delta



Extraction of oil and gas products from delta areas contributes to accelerated land subsidence. Data is from the USGS 2000 World Petroleum Assessment (40). Data is presented as aggregates over areas typically much larger than the deltas in this study. Rather than attempt to disaggregate this data, oil/gas extraction is treated as a binary flag to indicate only the presence of extraction activities.

Sea level rise trend
(ACI Component)

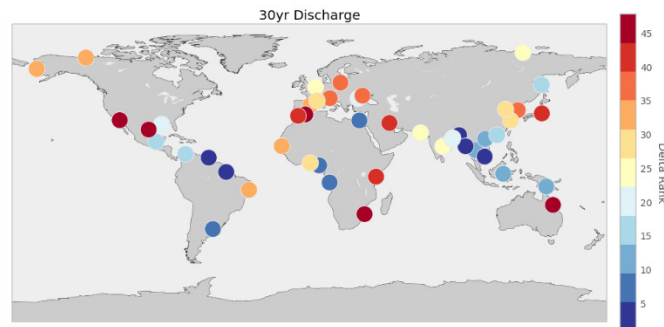
Delta



Sea level rise trend derived from the satellite altimetry record. Trends were calculated for each ocean pixel in the Church et al. (2004) dataset (42). Data was not adjusted for glacial isostatic adjustment, nor for the inverse barometric effect. Here, we are focused on the local sea level rise experienced at the coast, rather than total ocean volume, and so have included the effects of these processes in the data.

30yr river discharge
(HEI Component)

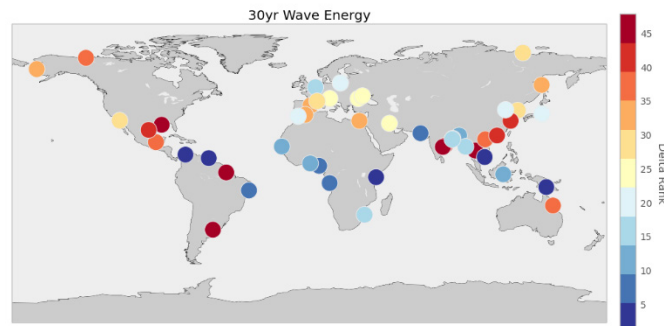
Delta



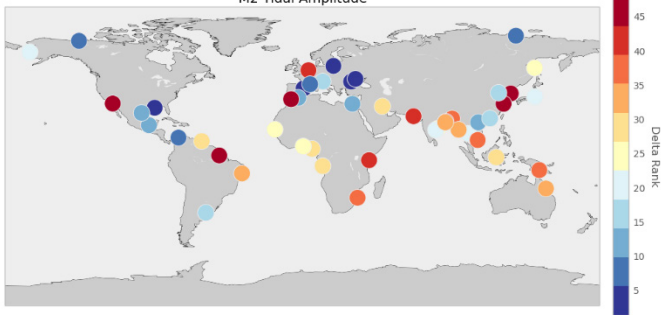
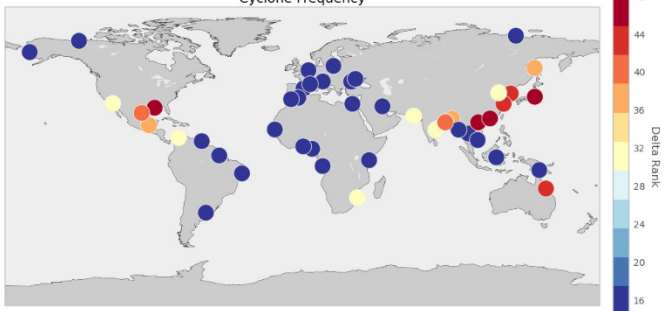
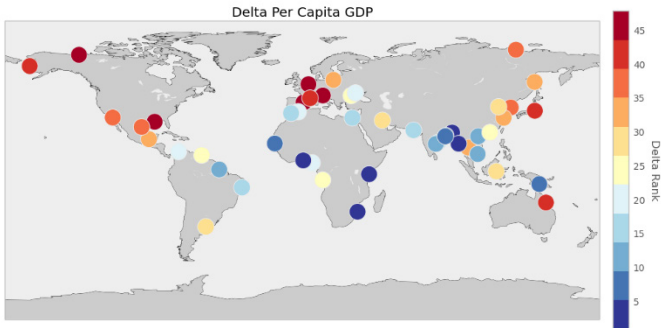
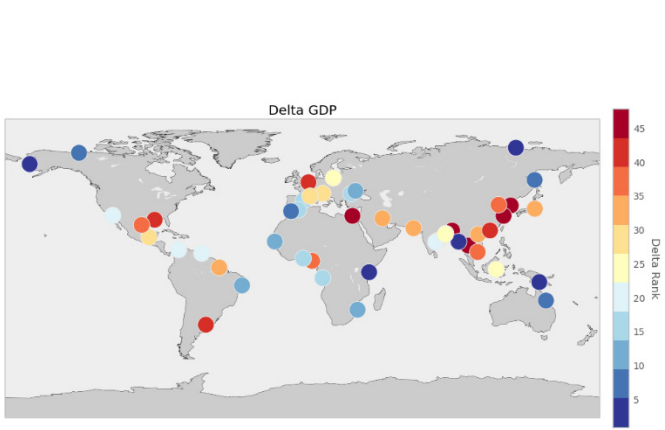
30 year return level of river discharge, from WBMplus model output (45). Return level is estimated by fitting a Generalized Pareto Distribution to data in the 99th percentile and higher, from a daily 1950-2012 hindcast simulation.

30yr wave energy
(HEI Component)

Delta



30 year return level of wave energy, from WAVEWATCH III model output (46). Return level is estimated by fitting a Generalized Pareto Distribution to data in the 99th percentile and higher, from a 3 hourly, downscaled to daily 1979-2010 hindcast simulation.

<p>M_2 tidal amplitude (HEI Component)</p>	<p>Delta</p> 	<p>Data from the OSU TPXO global tidal inversion (48). Higher tidal amplitude at a given delta increases the maximum possible storm surge.</p>
<p>Tropical Cyclone Frequency (HEI Component)</p>	<p>Delta</p> 	<p>Global index of tropical cyclone frequency based on empirical data from the Center for Hazards and Risk Research - Natural Disaster Hotspots database (47).</p>
<p>Per-capita GDP (IDI Component)</p>	<p>Delta</p> 	<p>Per-capita GDP, extracted from a global gridded GDP dataset (50). Higher per-capita GDP suggests stronger homes and other infrastructure that can better withstand a flooding event, reducing vulnerability.</p>
<p>Aggregate GDP (IDI Component)</p>	<p>Delta</p> 	<p>Aggregate GDP, extracted from a global gridded GDP dataset (50). High aggregate GDP across a delta suggests both a concentration of assets that are worth protecting, and also a financial base to invest in larger protective engineered structures such as levees, pumping stations, and storm surge barriers.</p>

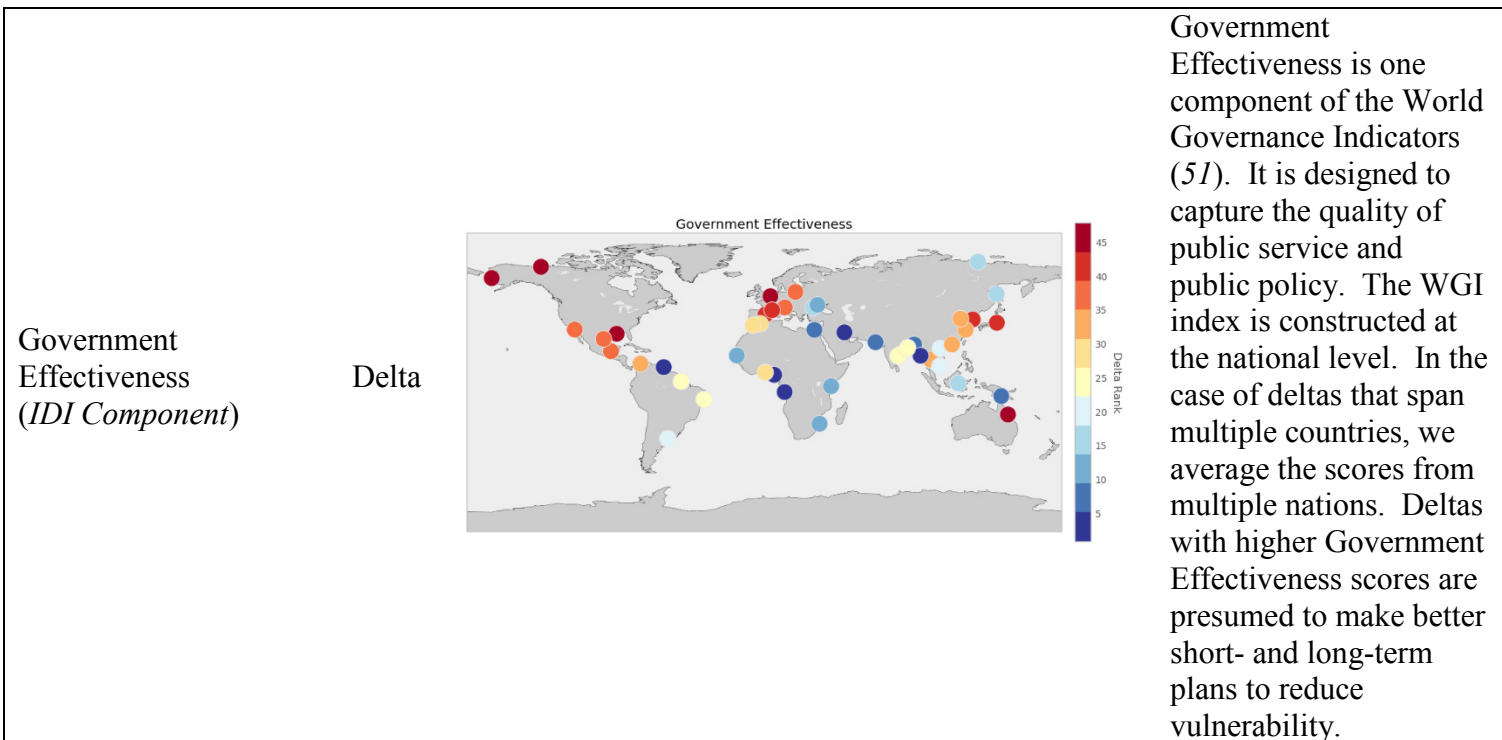
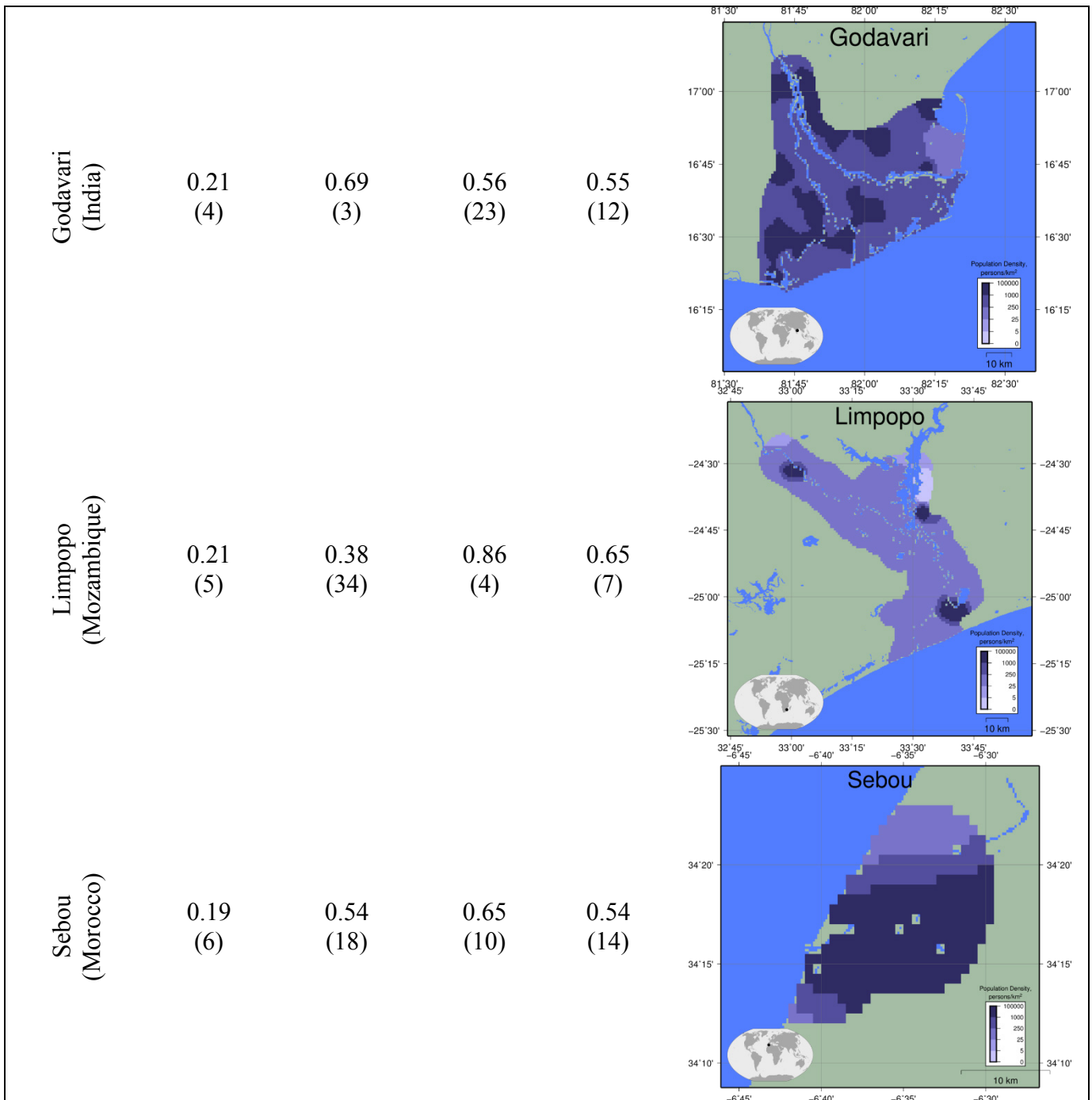
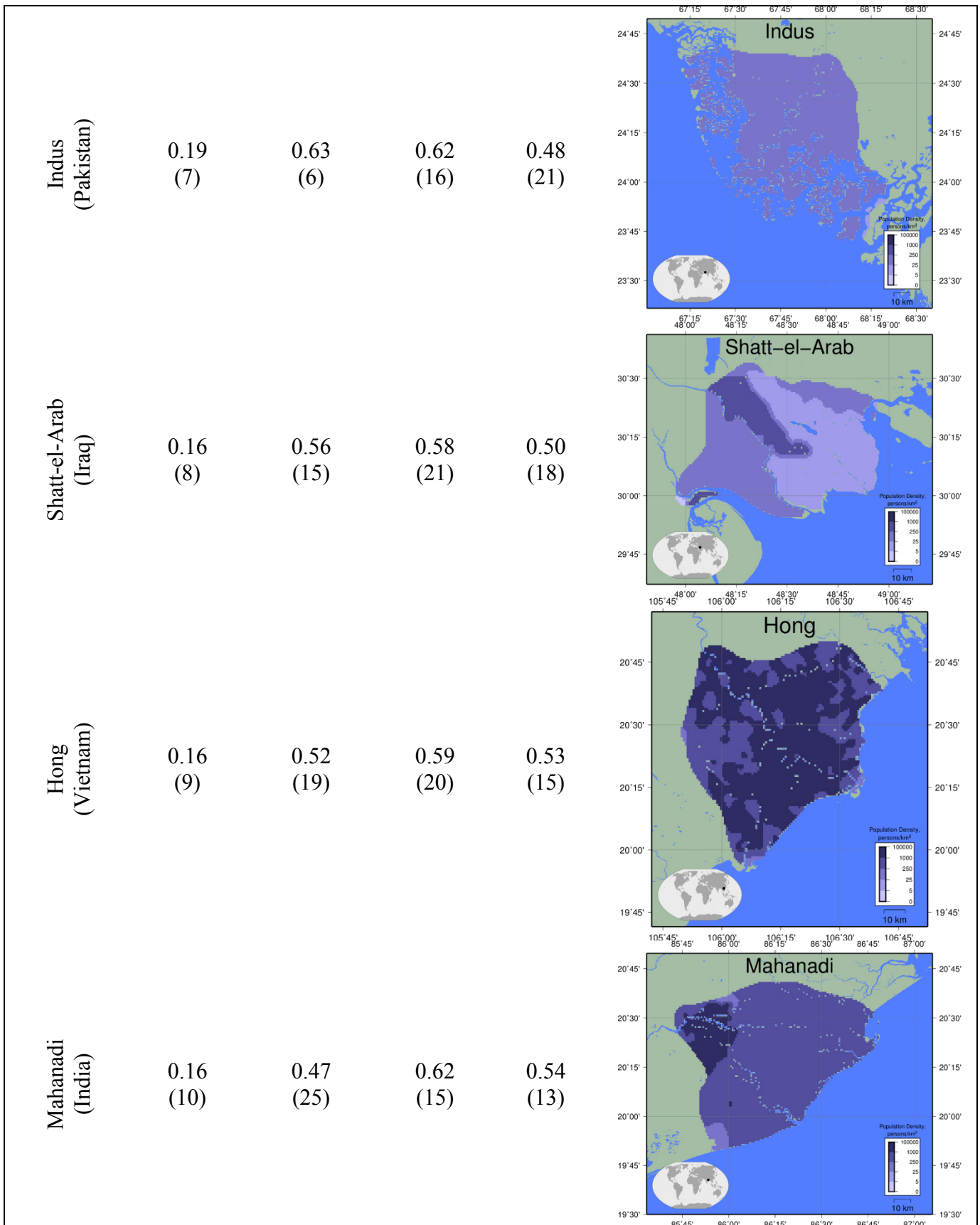
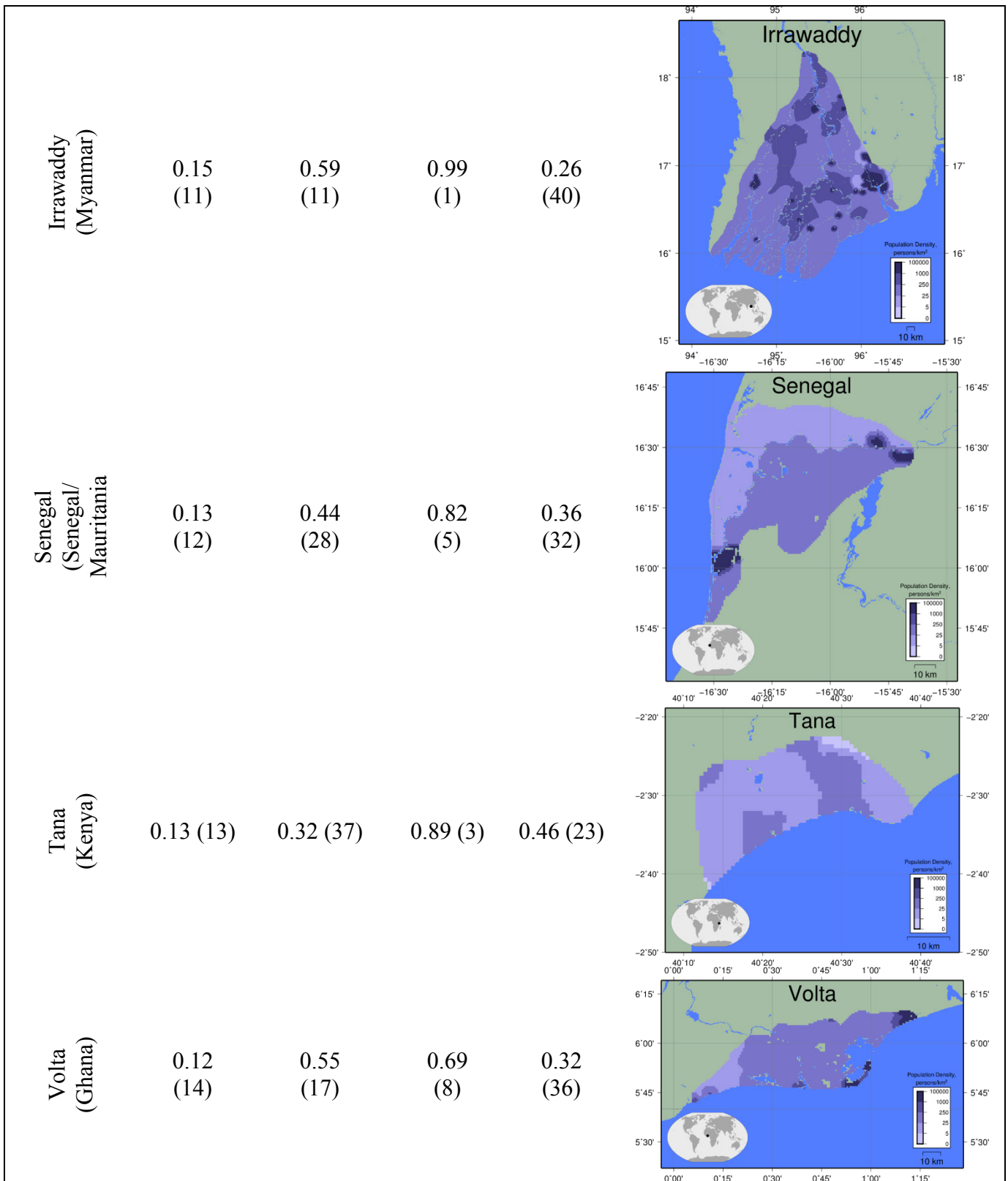


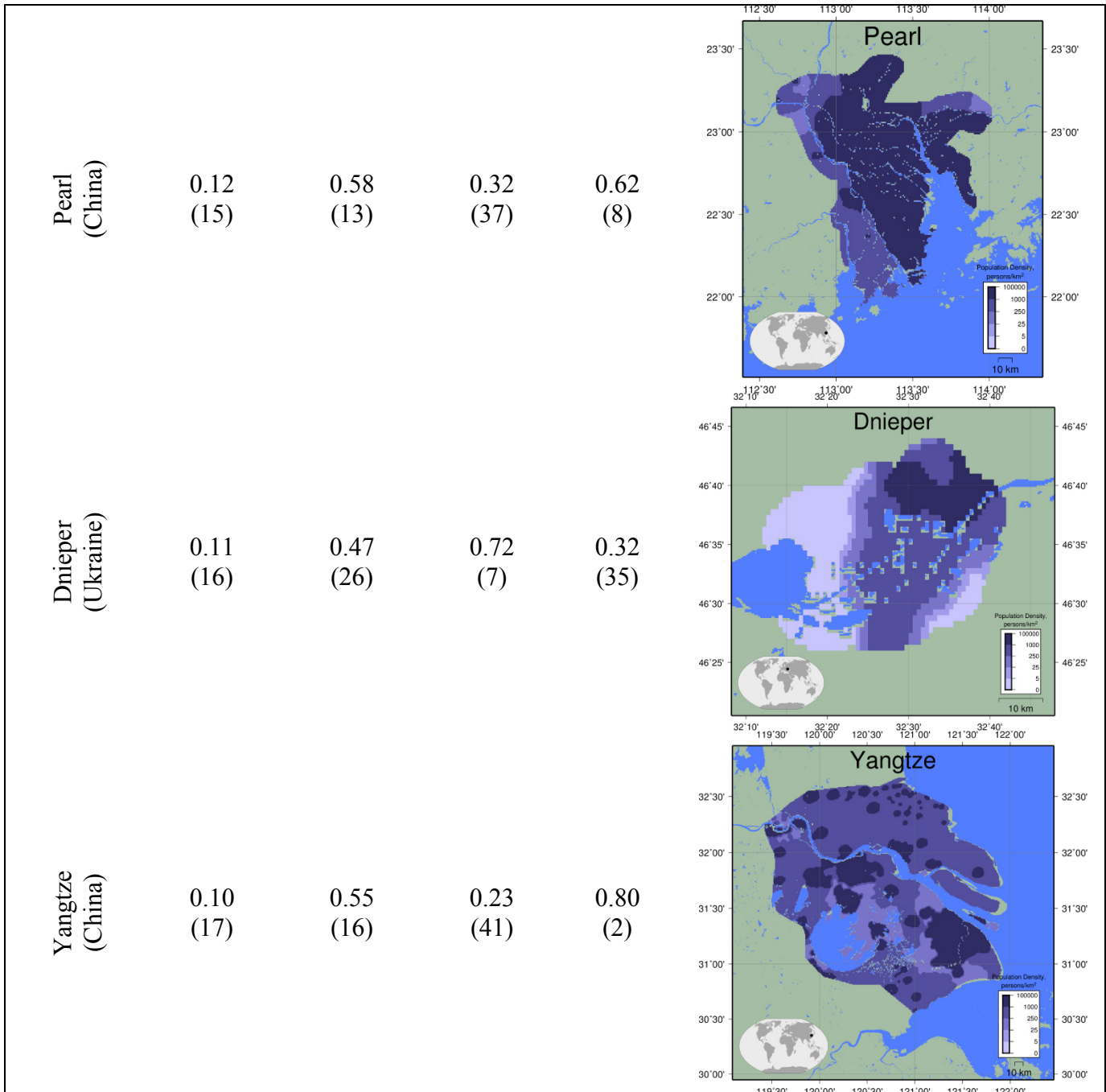
Table S1: Description and maps for each delta and basin indicator variable for the Anthropogenic Conditioning Index, Hazardous Events Index, and Investment Deficit Index.

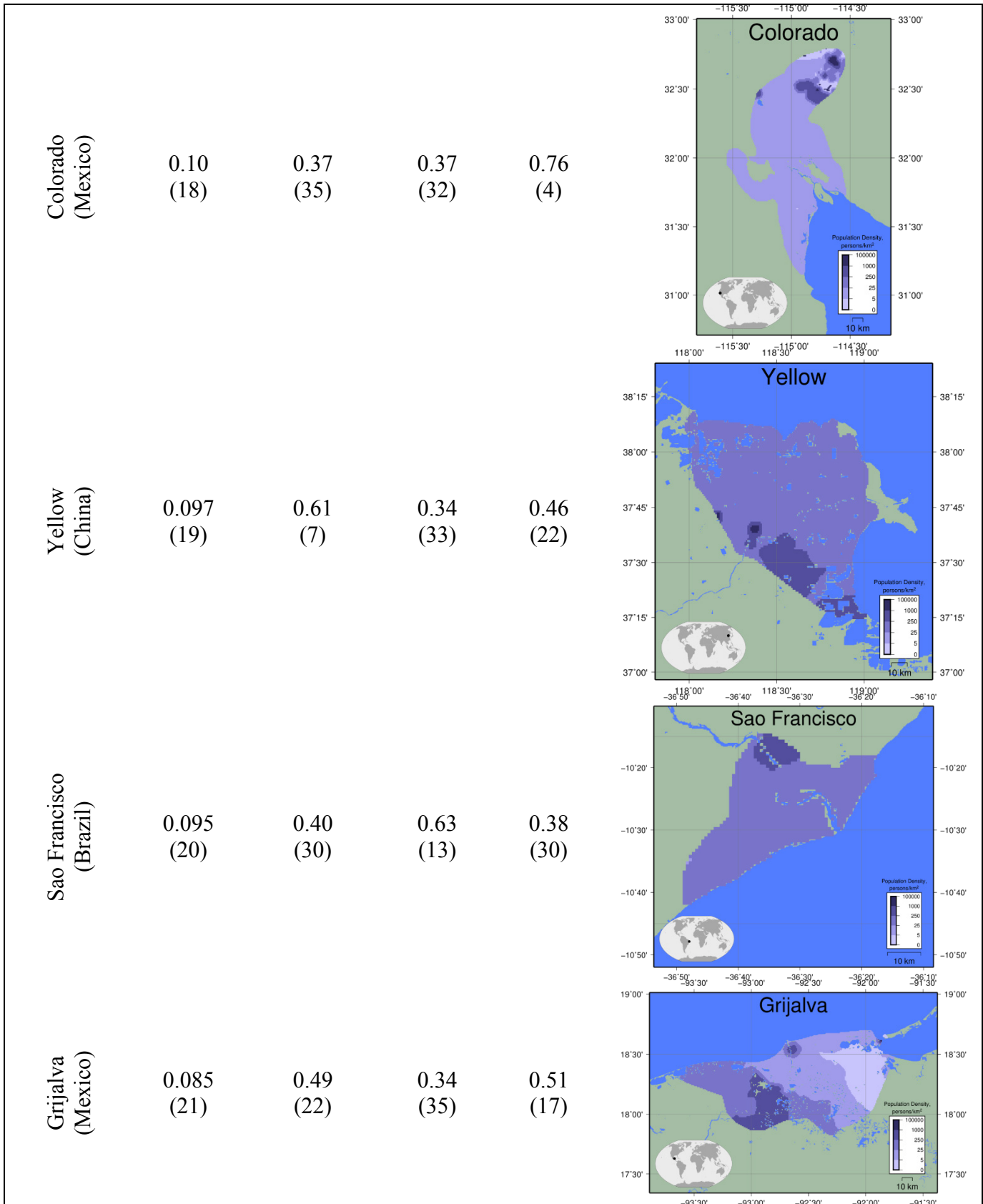
Delta (Country)	Risk rate of change index:	Anthropogenic Conditioning Index:	Investment Deficit Index:	Hazardous Events Index:	Delta extent map, with population
	\hat{R}' (rank)	\hat{E}' (rank)	\hat{V} (rank)	\hat{H} (rank)	
Krishna (India)	0.28 (1)	0.72 (2)	0.64 (11)	0.60 (9)	
Ganges-Brahmaputra (Bangladesh)	0.22 (2)	0.80 (1)	0.62 (16)	0.45 (24)	
Brahmani (India)	0.22 (3)	0.60 (9)	0.64 (12)	0.57 (11)	

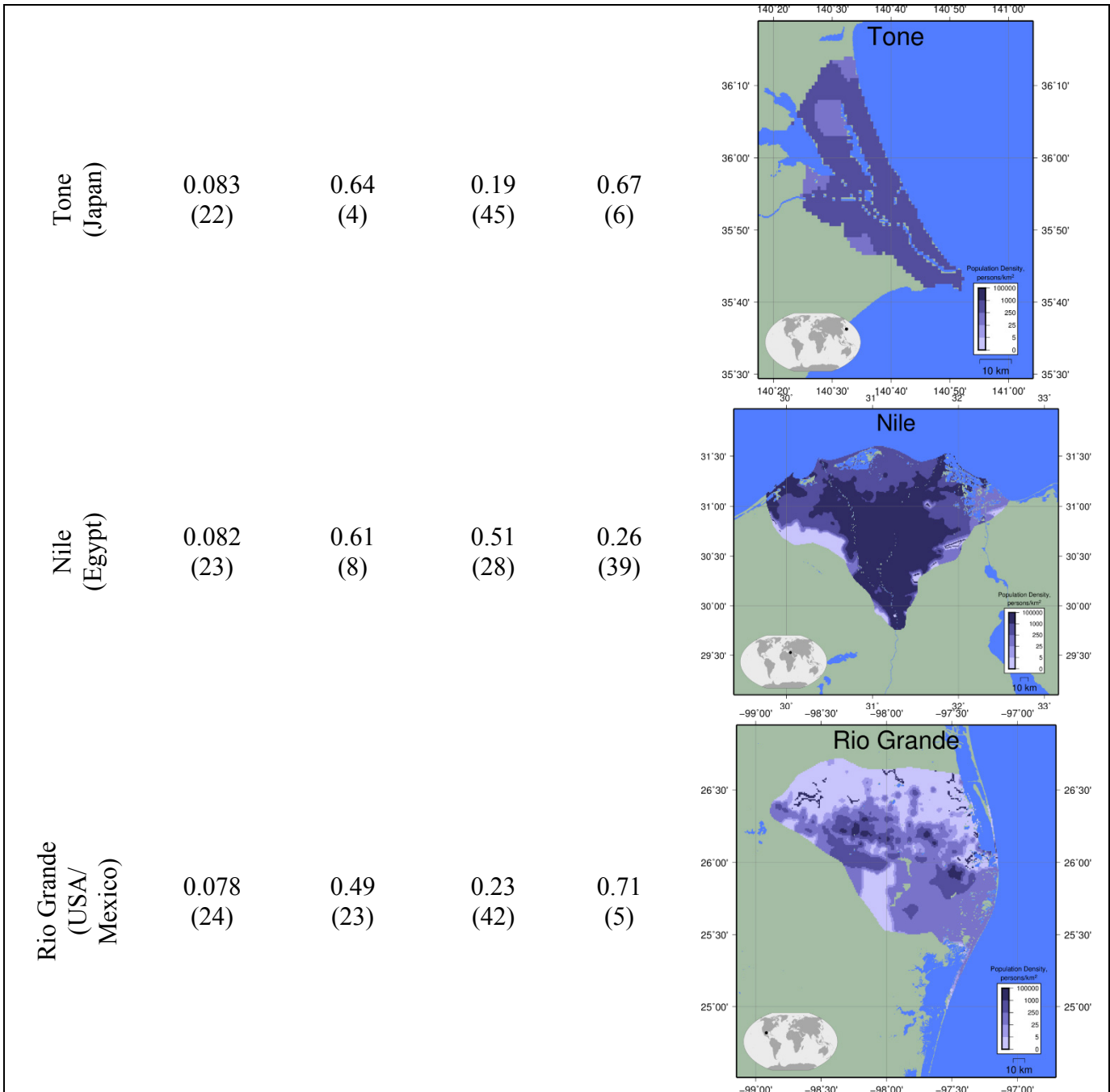


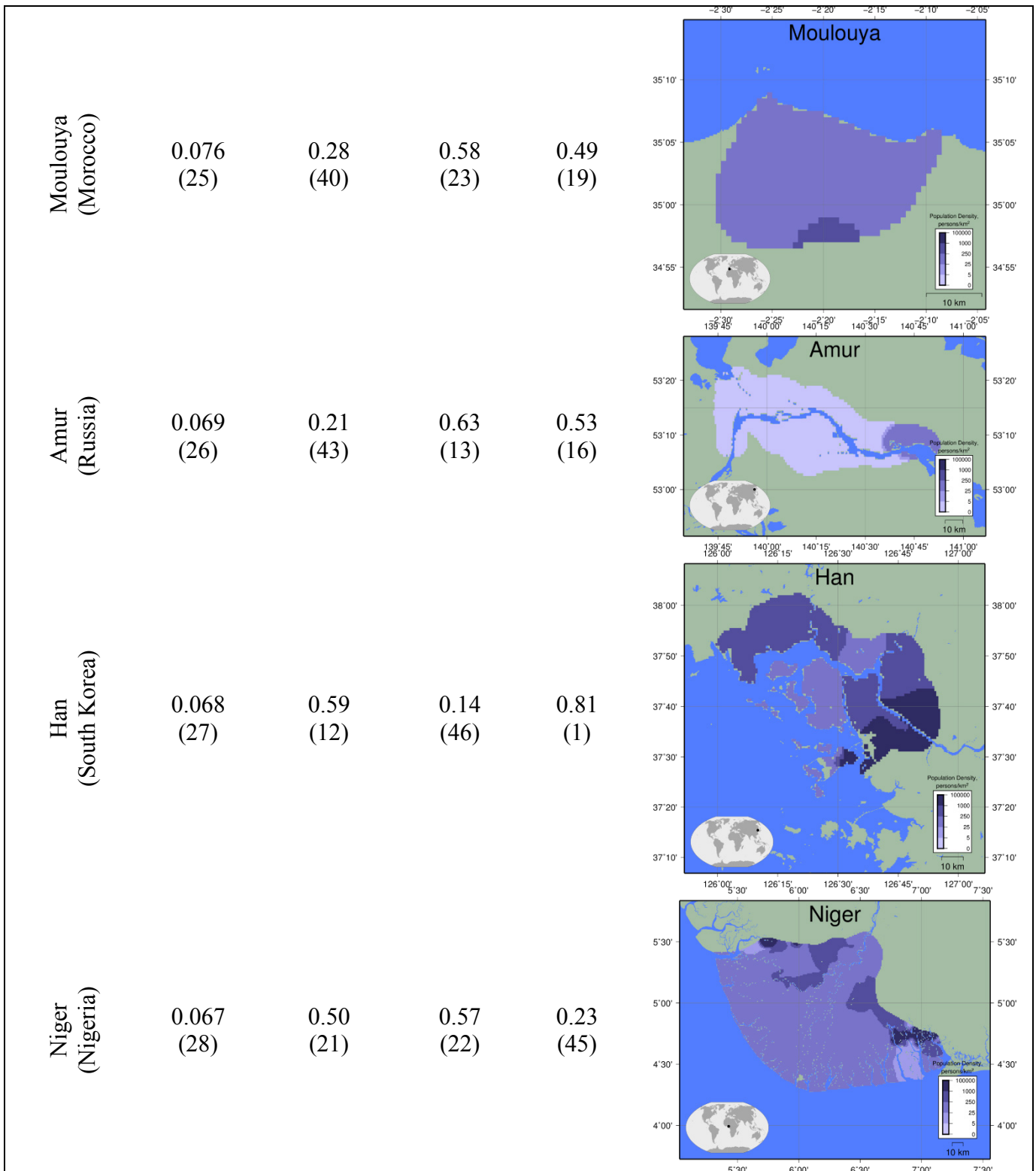






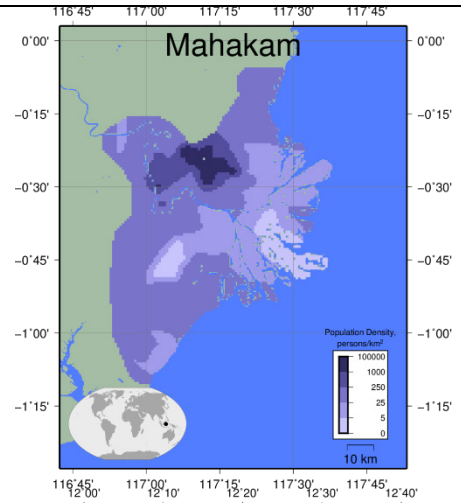






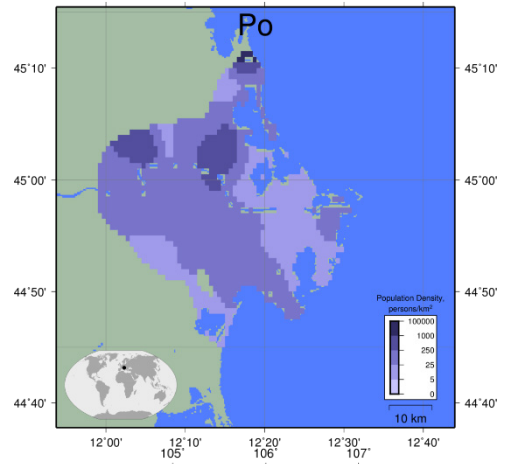
Mahakam
(Indonesia)

0.061
(29) 0.45
(27) 0.52
(27) 0.26
(41)



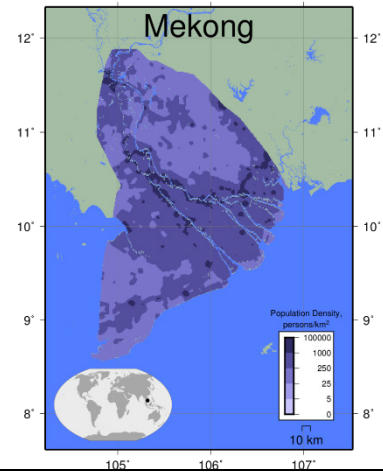
Po
(Italy)

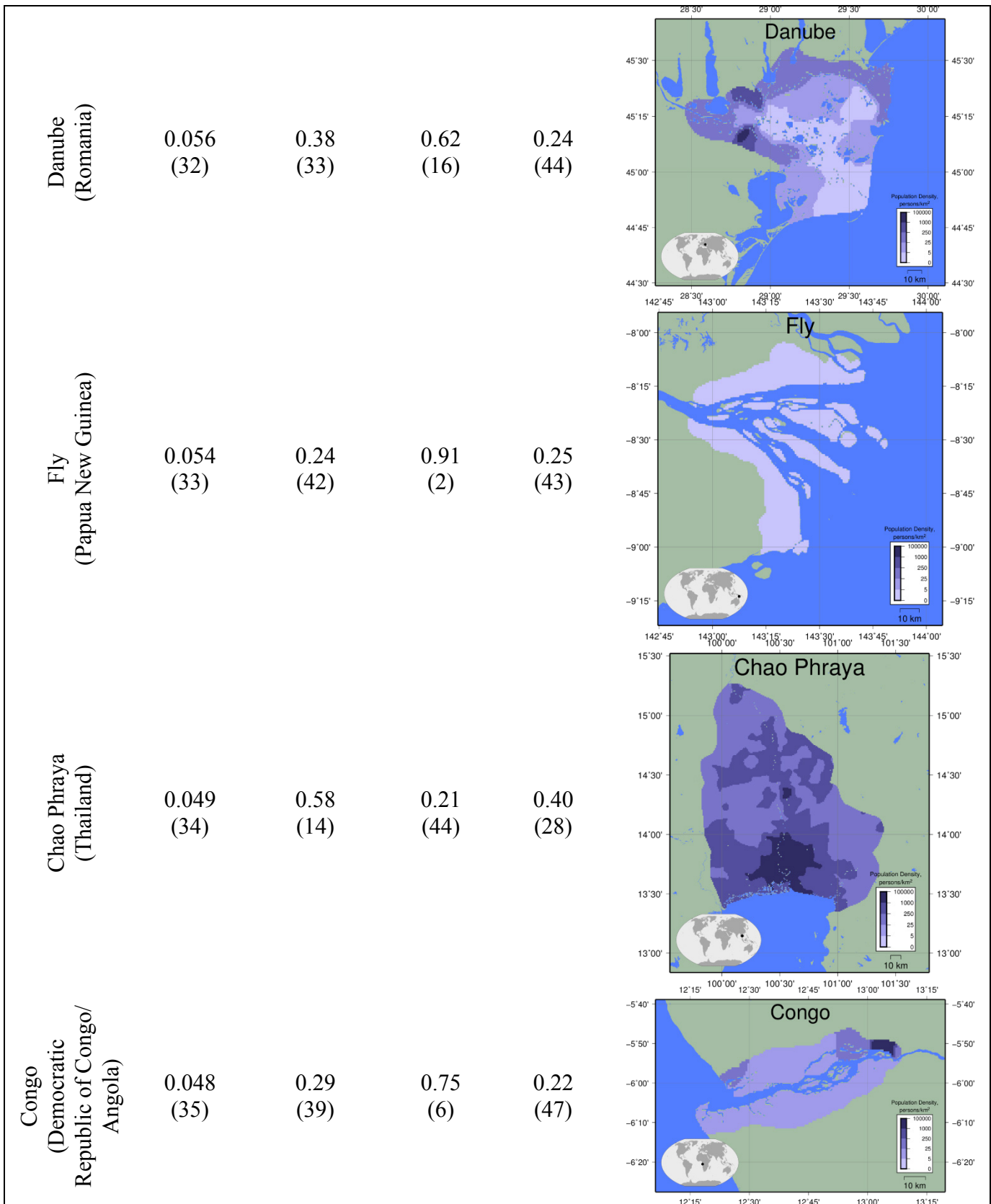
0.060
(30) 0.64
(5) 0.25
(40) 0.38
(29)

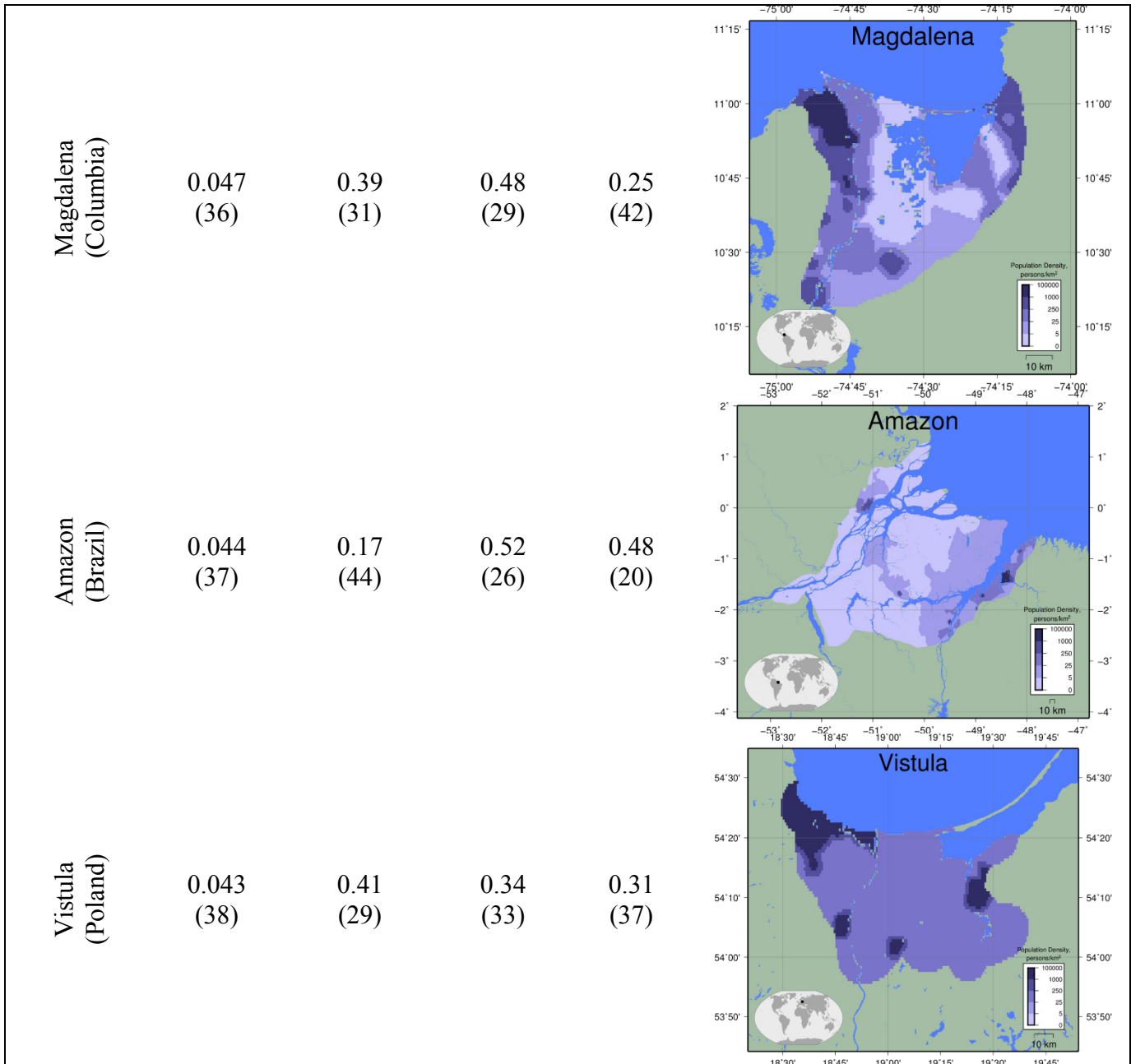


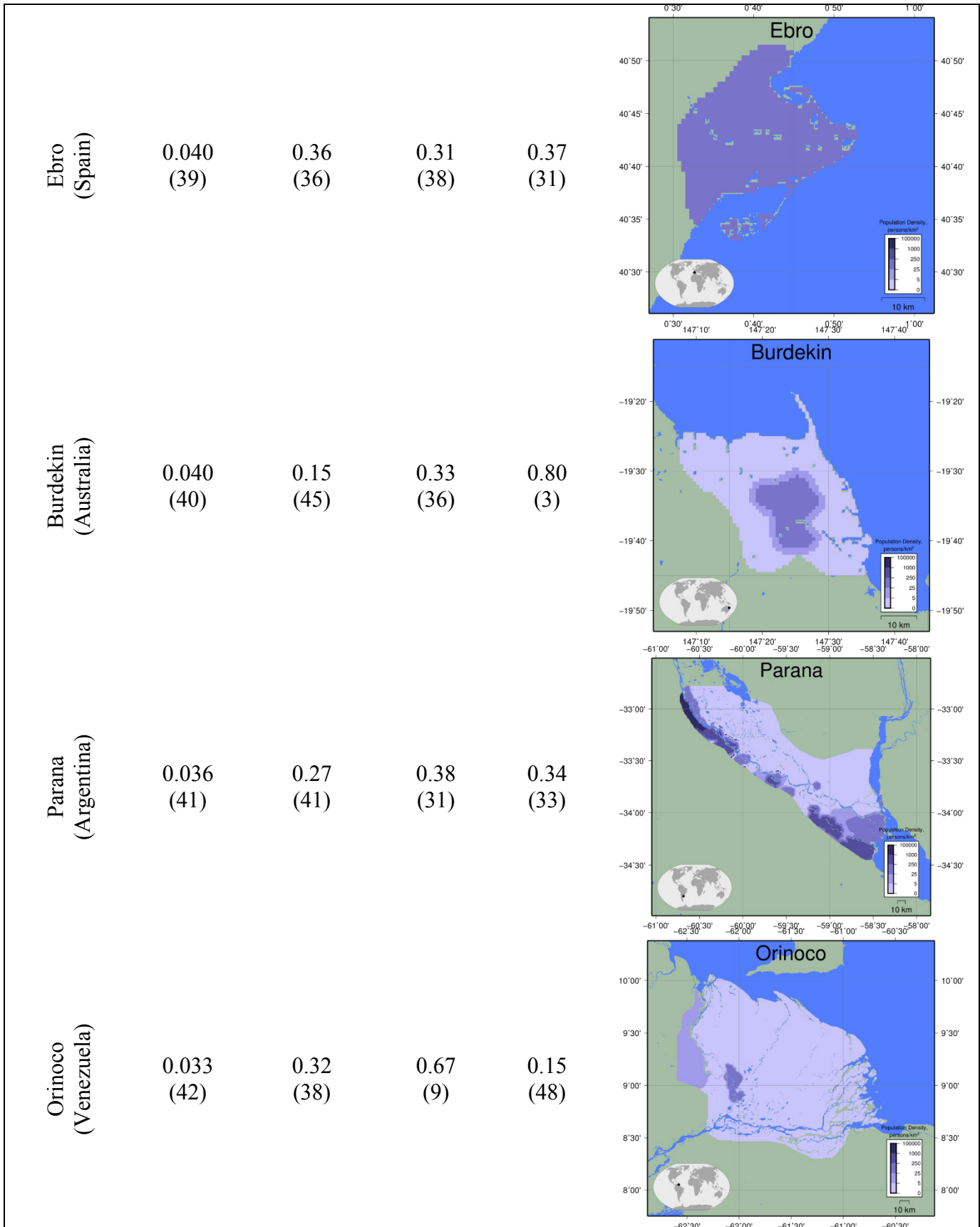
Mekong
(Vietnam)

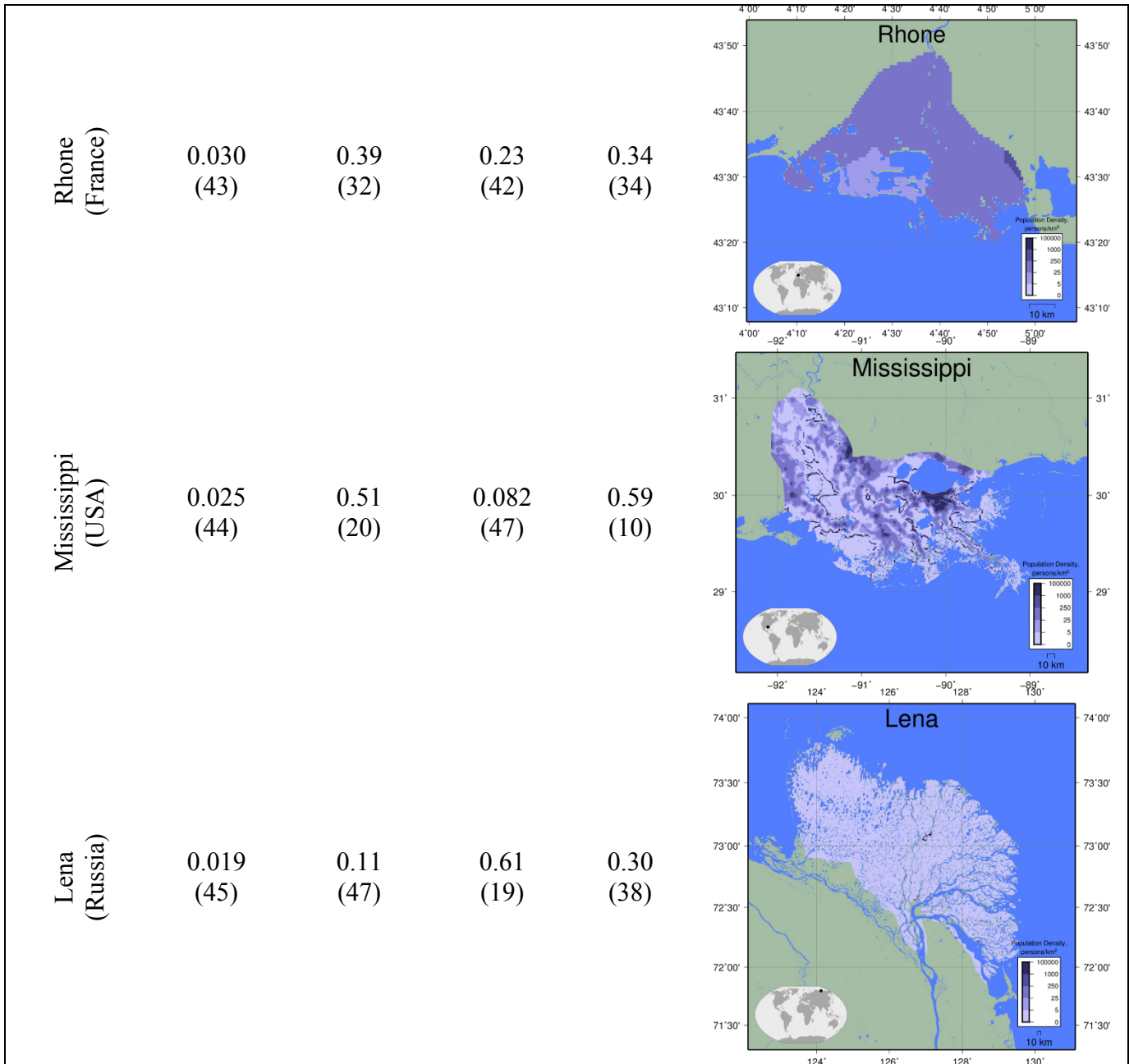
0.057
(31) 0.48
(24) 0.54
(25) 0.22
(46)











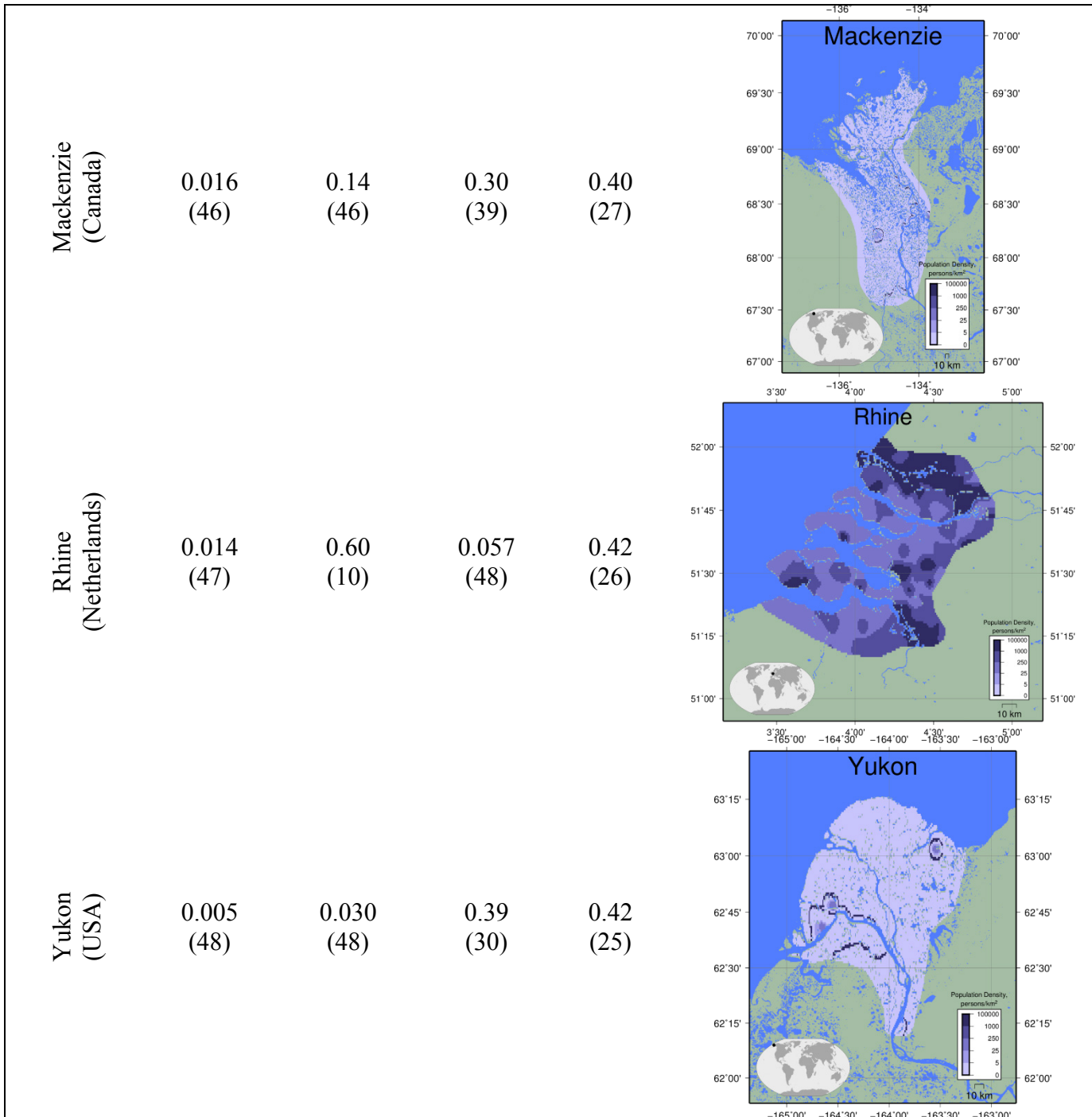


Table S2: Delta index scores, with ranks in parentheses, and population maps, ordered by increasing \hat{R}' . Maps show GRUMPv1 population density estimates, overlaid on MODIS MOD44W land/water mask (52).

	Low oil price scenario	Reference Case	High Oil Price Scenario
GDP Price Index	1.7%	1.8%	1.9%
Fuel and Power Wholesale Price Index	1.9%	2.9%	4.4%

Table S3: US Energy Information Administration *Annual Energy Outlook 2015* price index annual growth rates, forecasts for 2040 (28).